Ionics (2019) 25:3299–3307
https://doi.org/10.1007/s11581-019-02850-8

ORIGINAL PAPER

A hydrothermal carbonization process for the preparation of activated carbons from hemp straw: an efficient electrode material for supercapacitor application

Xia Jiang[1,2] · Gaofeng Shi[1] · Guoying Wang[1] · Puranjan Mishra[3] · Chao Liu[1] · Yucan Dong[1] · Peng Zhang[1] · Haoqi Tian[1] · Yanrong Liu[1] · Zhao Wang[1] · Qi Zhang[1] · Hongquan Zhang[1]

Received: 13 October 2018 / Revised: 29 November 2018 / Accepted: 22 December 2018 / Published online: 4 February 2019

Abstract

In the present study, a hemp straw activated carbon (HSAC) was simply prepared by hydrothermal process followed by a pre-oxidization and carbonization by KOH solid-state activation. The as-synthesized HSAC shows abundant porosity, which is designed to be beneficial to the fast transportation of electrolyte. The preparation conditions for HSACs under different mass ratios of KOH:precursors were optimized, and the sample obtained by a mass ratio of 4:1 showed an outstanding capacitive property (specific capacitance of 279 F g^{-1} at 0.5 A g^{-1} current density). Besides, the capacitance of 91.6% was retained after 5000 charge-discharge cycles under 2 A g^{-1} current density. The resulting symmetrical supercapacitor obtained by using the HSAC electrodes exhibited an excellent electrochemical performance, which successfully illuminated a LED light. The HSAC has great potentials as electrode material for high-performance supercapacitor, which opens a new way for value increment of natural products.

Keywords Hydrothermal method · Hemp straw · Activated carbons · Electrode material · Supercapacitor

Introduction

With the increasing concern for global energy depletion and environmental pollution, it is imperative to find out a clean, efficient, and sustainable source of energy, as well as new technologies associated with energy conversion and storage [1, 2]. The supercapacitors are energy storage devices that can be safely charged or discharged within a very short period of time with long cycle life [3]. These devices have emerged as promising candidates for flexible energy storage devices in a wide range of applications, including hybrid electric vehicles, mobile electronic devices, and distributed sensor networks, to name a few, due to its high-power density and simple structure [4, 5].

Supercapacitors are mainly composed of positive electrode, negative electrode, diaphragm, and an electrolyte. The electrode materials are one of the key components for supercapacitors; therefore, the development of efficient electrode materials is essential for construction of high-performance supercapacitors. At present, carbonaceous materials [6, 7], metal oxides [8, 9], conductive polymer materials, and composite materials [10, 11] have been extensively investigated as potential candidates for the electrode materials [12].

Primarily, the carbon materials are considered as most prospective electrode materials for industrialization, due to their easier availability, cost effectiveness, non-toxicity, large specific surface area, good conductivity, and excellent physicochemical stability [13]. To date, there are various kind of carbon materials, such as activated carbons [14], template carbons [15, 16], carbon nanofibers [17], carbon nanotubes [18], carbon aerogel [19], and graphene [20, 21], which have been commonly explored for electrode materials. Particularly, the activated carbons have been used widely as electrode materials for supercapacitors. The natural biomass–based carbon sources were recently used to synthesize carbon-based supercapacitors. Along with this line, different crude biomass such as reed straw [22], orange peel [23], Camellia oleifera

✉ Gaofeng Shi
gaofengshi_lzh@163.com

[1] School of Petrochemical Engineering, Lanzhou University of Technology, Lanzhou city, China

[2] Gansu Vocational College of Agriculture, Lanzhou city, China

[3] Faculty of Engineering Technology, Universiti Malaysia Pahang, Lebuhraya Tun Razak, Gambang, 26300 Kuantan, Pahang, Malaysia

shell [24], and lignocellulosic materials [25] had been employed as raw materials to produce porous carbons. These materials were prepared to show excellent performance as electrode materials in supercapacitors.

In this regard, hemp is one of the major crops in Western China and its straw remains left worthless in the harvested fields. Therefore, it is attracting a large amount of attention from the viewpoint of "waste-to-wealth" in different potential applications [26]. In existing research, Huanlei Wang et al. prepared carbon nanosheets with high-energy ultrafast supercapacitors by treating hemp with dilute sulfuric acid [27]. In our research group, carbon nanofibers were also prepared by hemp, which has high electrochemical performance [28]. Additionally, it exhibits interesting properties such as high porosity and loose structural features. Compared with other natural products, the inherently large porosity of hemp precursors could remain as unchanged after carbonization treatment. Such resulting carbon originated from hemp with abundant porosity should be of great importance for fast transportation of mass for their electrochemical applications. Based on this view of point, in this work, we report the synthesis of the hemp straw activated carbon (HSAC) electrodes by hydrothermal process followed by a pre-oxidization and carbonization by KOH solid-state activation. As a proof-of-concept study, the as-synthesized HSAC shows high capacitance, rate capability, and cyclic stability, which hold great potential as promising electrode materials for supercapacitors, by in combination with their low-cost and environmentally friendly production process.

Experimental

Materials

All the chemicals used in this present work were analytical reagent (AR) grade. The hydrogen peroxide (H_2O_2), acetic acid (HAc), potassium hydroxide (KOH), and hydrochloric acid (HCl) were purchased from Chemical Reagent Co., Ltd. All reagents were directly used without further purification. Deionized water was used.

Synthesis of carbon materials

The hemp straw was procured from Gansu, China. Briefly, the hemp straw was repeatedly washed with deionized water to remove dust and impurities and then dried in an oven at 80 °C for 24 h. The resulting dried hemp straw was crushed to powder of particle size below 100 meshes. Thereafter, 1.0 g of hemp straw powder and 50 mL of H_2O_2-HAc aqueous solution were hydrothermally treated in a Teflon-lined stainless steel autoclave (100 mL) at 120 °C for 4 h. Finally, the suspension was centrifuged and freeze-dried.

Then, the as-prepared white powdered sample was mixed with KOH in different mass ratios and crushed in an agate mortar for 20 min, followed by heating at 800 °C for 1 h and the heating ratio is 3 °C per minute in N_2 gas atmosphere. Thereafter, the activated carbon samples were thoroughly washed with 10 wt% HCl solution. Eventually, the carbons were dried at 80 °C for 12 h in an oven. The samples were named as HSAC-*X*, where HSAC is hemp straw activated carbon and *X* (*x* = 0, 2, 3, 4, 5, or 6) stands for the mass ratio of as-prepared powder:KOH. For analysis and comparison, the as-prepared samples which the HAC-H_2O_2-treated sample is named as HSAC-a.

Structure characterization

A field emission scanning electron microscope (SEM, JSM-6701F, Japan) was used to characterize the morphology of the HSAC-*X*. The specific surface area was measured by using the Brunauer-Emmett-Teller method by N_2 adsorption and desorption at 77.3 K using a volumetric sorption analyzer (BET micromeritics ASAP 2020). The crystal structure was analyzed by an X-ray diffraction (X'Pert Powder, Dutch PANaly) in the 2θ range of 5 to 80°. Raman spectrum was evaluated by a spectrometer (JYHR800, Micro-Raman). Surface composition was tested with an X-ray photoelectron spectroscope (XPS, PHI5702, USA).

Test of electrochemical properties

The electrochemical measurements of carbon electrodes were carried out by using CHI660D electrochemical work station (CHI660D, Shanghai Chenhua Instrument Co. Ltd.) in 6 mol L^{-1} KOH aqueous solution. The standard three-electrode system containing platinum plate as counter electrode and as reference electrode saturated calomel electrode. The activated carbon material was mixed with carbon black and PTFE with a mass ratio of 85:10:5 in ethanol to form slurry for the preparation of electrodes. The slurry was coated on nickel foam current collector with coating area of 1 cm^2 and dried at 80 °C for 12 h in a vacuum oven. The electrochemical test includes cyclic voltammetry (CV), galvanostatic charge-discharge (CP), and alternating current impedance (EIS). For a three-electrode configuration, specific capacitance of the electrode materials was calculated by Eq. (1):

$$c = \frac{I\Delta t}{m\Delta V} \tag{1}$$

where I is the discharge current (A), Δt is the discharge time (s), m is the mass of electrode (g), and ΔV is the voltage window (V) [29].

Symmetric supercapacitor cells were assembled using the fabricated ACs as electrode materials and 6 mol L^{-1} KOH

solution as electrolyte. The AC material was mixed with carbon black and PTFE with a mass ratio of 85:10:5 in ethanol to form slurry for the preparation of electrodes, and then pressed onto a nickel foam that served as a current collector. The electrodes fitted with the separator (PP/PE complex film) and electrolyte solution were symmetrically assembled into electrode/separator/electrode construction (sandwich-type cells). The capacitance (C) of the electrode also can be calculated by Eq. (2):

$$C = \frac{4(I\Delta t)}{m\Delta V} \tag{2}$$

where I refers to the applied current density (A), Δt and ΔV present the discharging time (s) and potential range after the IR drop (V), respectively, and m (g) is the total mass of electrodes [30].

Results and discussion

Structural characterization

The scanning electron microscopy analysis was used to display the microstructures of hemp straw, HSAC-a, and HSAC-4 (Fig. 1). It can be clearly seen that the powder of hemp straw exhibited loose, flaky, and regular pores, which significantly differ from other biomass sources, so it is a good source of carbon material due to its unique structural characteristics (Fig. 1a). After the addition of H_2O_2 and HAc, the structure of hemp straw was changed to comparatively thinner sheet-like structures due to the oxidation of H_2O_2 and the hydrolysis of HAc (Fig. 1b). So we can see that the cellulose unites in hemp receptacle are partly oxidized by an oxidant (H_2O_2) for pores and further hydrolyzed in a weak acid (HAc) to effectively exfoliate the polymer from aggregative bulks into nanocellulose sheets, which is consistent with previous literature reports [31].

Activation is an effective way to create porosity, to widen existing pores, or to modify the surface of pores. Two types of activations are used, namely physical and chemical activations. During chemical activation process, the actions between activation reagents like potassium hydroxide, zinc chloride, or phosphoric acid and carbon usually occur at certain temperatures, which allows one to better control to increase the surface area and improve the electrochemical performance [32].

So we used KOH as activation reagents when the activation temperature is higher than 400 °C. The chemical reactions are involved into the process, K_2CO_3 forms at about 400 °C, and KOH is completely consumed at about 600 °C if carbon is sufficient. At a temperature higher than 700 °C, K_2CO_3 decomposes into CO_2 and K_2O [33].

The chemical reactions are involved into the process:

$$6\,KOH + 2\,C \rightarrow 2\,K + 3\,H_2 + 2\,K_2CO_3,$$
$$K_2CO_3 + 2C \rightarrow 2K + 3CO,$$
$$K_2O + 2C \rightarrow 2K + CO$$

In our study, we screened the best mass ratio of prepared powder:KOH, we found that when the prepared powder mass ratio:KOH is 4:1, HSAC-4 has the optimum pore distribution. The KOH activation changes the chemical character and the porous structure of the hemp; it is clearly seen that pores have been generated on HSAC, which might have influenced on its electrochemical capacitive performance capacity. Holes of different sizes were created after pre-oxidation and carbonization; the original large micron-sized pores has not been destroyed (Fig. 1c). All of these porous structures make great contributions to capacitive performance.

The N_2 sorption isothermal analysis was employed to further investigate the structure of the HSAC-4 samples. As illustrated in Fig. 2, N_2 isothermal adsorption/desorption curves of HSAC-4 belong to type 4 kind of isotherms, indicating different pore sizes from micropores to mesoporous structures [34]. The pore diameter distribution curves of HSAC-4 are in accordance with corresponding N_2 isothermal adsorption curves, from Fig. 2b. The surface area of HSAC-4 (865 $m^2\ g^{-1}$) was superior to HSAC (201 $m^2\ g^{-1}$) and HSAC-3 (527 $m^2\ g^{-1}$), whereas the average pore diameter of HSAC-4 (2.44 nm) was less than that of HSAC (4.2 nm) and HSAC-3 (2.9 nm). Therefore, the HSAC-4 shows an improved surface area than others, which indicates microporous structures play an important role in increasing the capacitive performance of porous carbon materials.

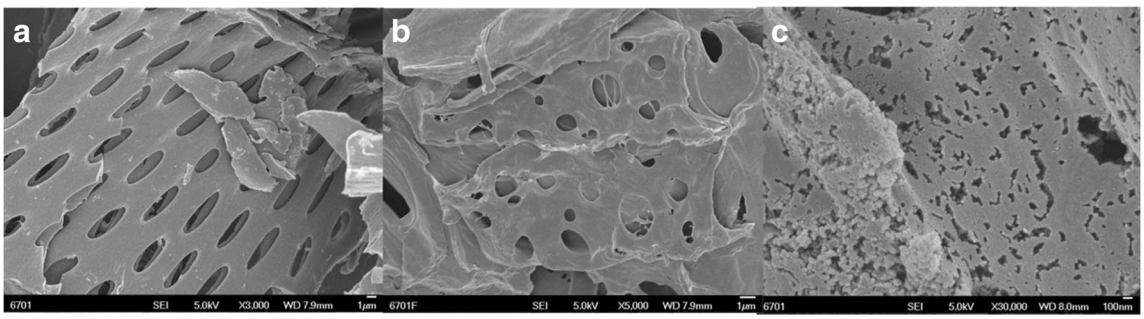

Fig. 1 SEM images of **a** hemp straw, **b** HSAC, and **c** HSAC-4

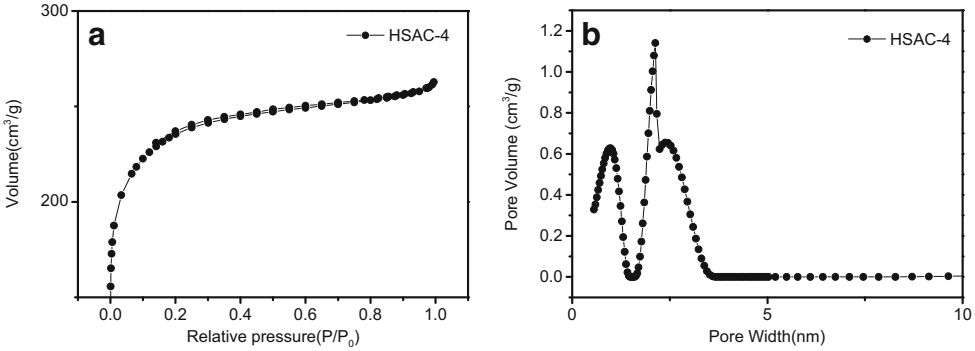

Fig. 2 **a** N_2 adsorption/desorption isotherms of samples. **b** Pore size distributions of HSAC-4

Figure 3a shows the typical FT-IR spectrum obtained for HSAC, HSAC-0, and HSAC-4. Three major characteristic bands at 1051, 1633, and 1739 cm^{-1} can be assigned to C–O stretching. The absorption peaks at 3420 cm^{-1}, 2895 cm^{-1}, and 1593 cm^{-1} are respectively assigned to –OH, –C-H, C=C, and C–O stretching vibrations on the surface of the HSACs [35]. The HSACs have the same absorption peaks, which indicate that they have the same oxygen functional groups on the surface. But HSAC-4 after high temperature carbonization has weakened absorption peak. Through further analysis, H_2O_2 or HAc though hydrothermal reaction process can increase the oxygen-containing functional groups of the matrix, although these oxygen-containing functional groups are weakened after high temperature carbonization.

XPS analysis was performed to study the elemental composition and chemical state of the as-prepared samples. We can observe from Fig. 3b that HSAC mainly consists of C, O, and N elements. The proportions of C, O, and N in HSAC are 88.24%, 10.15%, and 0.97% (atomic %) respectively. According to the analysis of XPS in Fig. 3c, it shows four

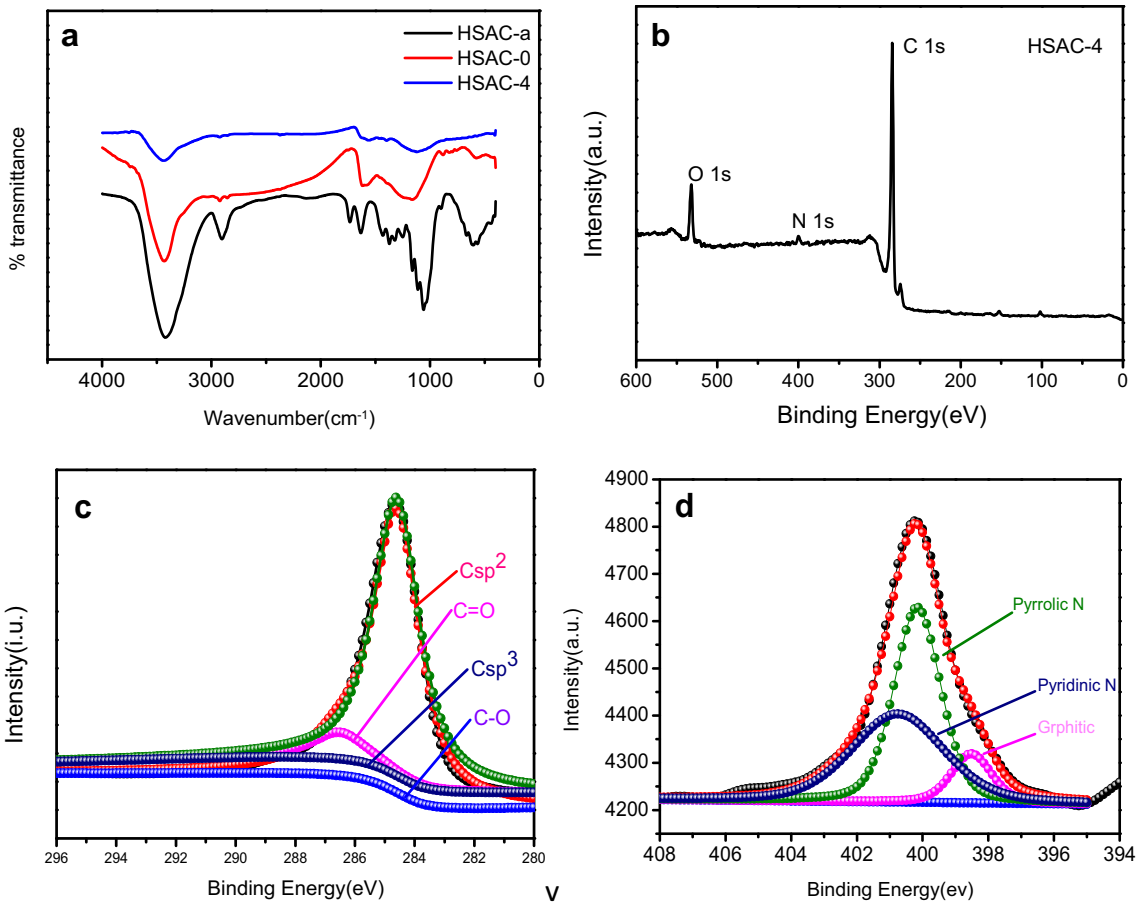

Fig. 3 **a** FT-IR spectra of the HSAC, HSAC-0, and HSAC-4. **b** XPS survey spectra of HSAC-4. **c** The C1s XPS spectra of HSAC-4. **d** The N1s spectra of HSAC-4

peaks at 284.65, 285.47, 286.54, and 287.8 eV, which belong to sp^2-bonded carbon, sp^3-bonded carbon, C–O, and C=O (carbonyl), respectively [36]. That is same as FT-IR spectrum analysis. Figure 3d displays that the N1s spectrum of HSAC-4 can fit well with three kinds of N species. Peaks at 398.3, 399.9, and 402.3 eV correspond to pyridine N, pyridinium N, and pyridine N-oxide, respectively [37]. It implies that the element N comes from the hemp straw precursor.

To further examine the structures of the samples, XRD characterization is shown in Fig. 4a. There are HSAC-0 and HSAC-4 in this Fig. 4a; they all display two obvious diffraction peaks. There is a broad peak located at $2\theta = 22.48°$ of HSAC-4 that corresponds to the (002) diffraction, indicating the presence of disordered carbon structure. The peak at $2\theta = 42.64°$ attributes to the (101) crystal planes of sp^2-C. The broad peak of HSAC-0 is at $2\theta = 23.34°$, while the peak is at $2\theta = 43.65°$. It was concluded that all samples synthesized by the hydrothermal carbonization process exhibit high graphitization of strong characteristic diffraction peaks from hemp straw, and the HSAC-4, which is a KOH-activated samples, has a relatively high degree of graphitization that is the (002); peaks obviously shift to the lower angle comparison with HSAC-0. According to the Bragg equation, $2d\sin\theta = n\lambda$, the interlayer spacing of the HSAC-4 is d002 = 0.39 nm. This value is larger than the distance between the graphite layers (0.335 nm), indicating that specifies an enlarger interlayer distance of the carbon [38].

The further characterization of the structures of "HSAC-4" using Raman spectroscopy is illustrated in Fig. 4b; the samples exhibited the three typical bands, that is, the G band (1338 cm^{-1}), D band (1587 cm^{-1}), and 2D band (2879 cm^{-1}). It is well known that the D band is closely related to the disorder-induced scattering resulting from imperfections or the loss of hexagonal symmetry of the carbon nanostructures, while the G band is related to the vibration of sp^2-bonded carbon atoms in a two-dimensional (2D) hexagonal lattice [39]. The intensity ratio between the G and D bands (I_G/I_D) is proportional to the graphitization degree of carbon materials. The sample demonstrated a high I_G/I_D value of 1.2, indicating a relatively high degree of graphitization which the result is agrees well with XRD. It is caused by its crt1ystallinity structure, which is good for the fast transmission of electrolyte ions, thus promoting ion diffusion and improving the capacitive performance of the porous carbon material.

Electrochemical characterization

To validate the promising applications, the electrochemical performances of HSACs were evaluated in a three-electrode system. Cyclic voltammetry (CV) curves for six different HSACs in Fig. 5a, which were tested between − 1 and 0 V at 5 mV s^{-1}, show no obvious redox peaks, which reveal that all HSACs mainly possess double-layer capacitances, and HSAC-4 has the largest CV-circulated area with a rectangular shape; thus, it has the highest double-layer capacitance among all six materials.

Figure 5b shows the CV curves of HSAC-4 at various scan rates from 5 to 100 m V s^{-1} between − 1 and 0 V; the CV curve still maintained a rectangular-like shape, indicating that HSAC-4 has good super capacitance characteristics at different scanning speeds. Figure 5c shows the galvanostatic charge-discharge curves for the HSACs at a current density of 0.5 A g^{-1}. They all display typical capacitor triangle shapes. According to Eq. (1), the calculated specific capacitances in terms of the charge-discharge curves are 137, 217, 193, 279, 189, and 92 F g^{-1} for HSAC-0, HSAC-2, HSAC-3, HSAC-4, HSAC-5, and HSAC-6, respectively. HSAC-4 has the highest value, much larger than the other five HSACs. It is clear that the capacitance performance of HSAC-4 is the best, which is consistent with the CV curves. This is also consistent with the previous structural analysis, HSAC-4 has the best pore distribution.

HSAC-4 at different current densities also exhibits a shape of nearly symmetrical triangle as illustrated in Fig. 5d, which is in consistent with the CV measurements. Even at current densities up to 10 A g^{-1}, the curve shows a close to an isosceles triangle shape, revealing a close to ideal capacitive behavior. Figure 5e shows the variation rate performances of the six samples. The specific capacitance of the samples decreased as the current density increased. We can see that the current density of the HSAC-4 is 279 F g^{-1} at 0.5 A g^{-1} and 220 F g^{-1} even at 10 A g^{-1}, a retention rate up to 78.9%, which means it maintains better stability throughout the charge-discharge test.

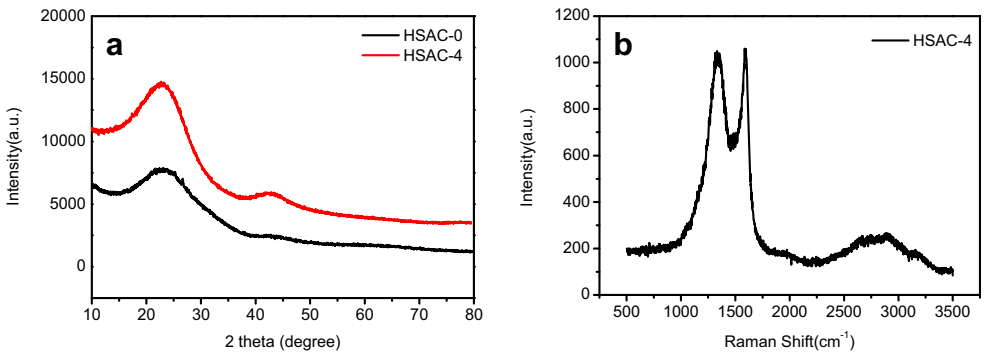

Fig. 4 **a** XRD patterns for HSAC-0 and HSAC-0. **b** Raman spectra of HSAC-4

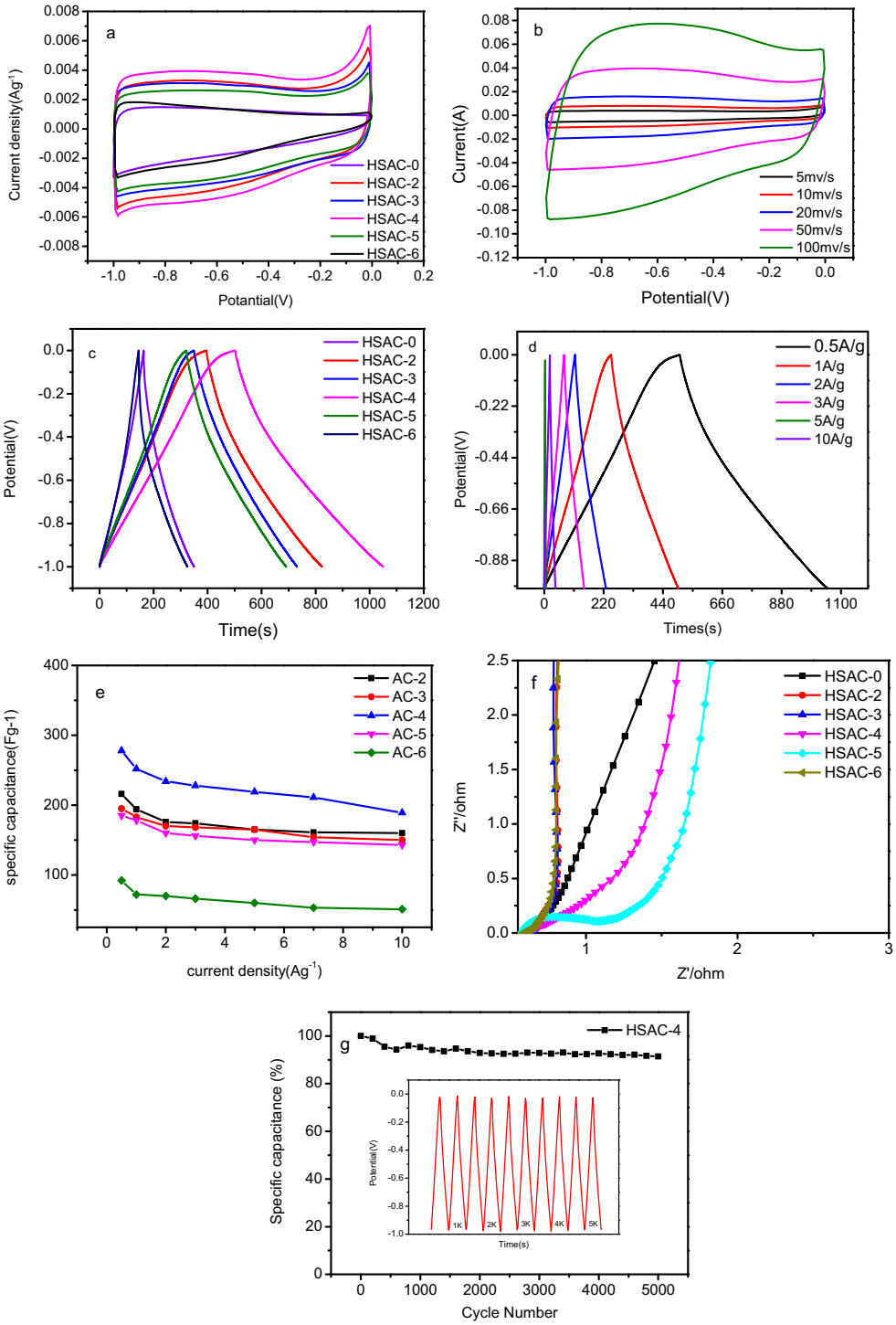

Fig. 5 Electrochemical performance of the samples measured in a three-electrode system. **a** CV curves for all the samples at a scan rate of 5 mV s^{-1}; **b** CV curves for HSAC-4 at scan rates ranging from 5 to 100 mV s^{-1}; **c** galvanostatic charge-discharge curves of all the samples at the current density of 0.5 A g^{-1}; **d** galvanostatic charge-discharge curves of HSAC-4 at different current densities; **e** specific capacitance of the samples versus various current densities from 0.5 to 10 A g^{-1}; **f** electrochemical impedance spectra (EIS) of the HSACs; **g** HSAC-4 in specific capacitance retention rates at the current density of 2 A g^{-1} after 5000 cycles

To get a deep insight of the electrochemical performance of the HSACs, EIS measurements were performed; the result is shown in Fig. 5f. In the high-frequency region, the point intersecting the real axis reflects the internal resistance (Rs) of the electrode material, and the semicircle corresponds to the charge transfer resistance (Rct). The nearly vertical line in the low-frequency region represents the diffusion resistance (*W*) of the electrolyte in the porous structure [40]. The curves of these samples have small radii in the high-frequency region and tend to be straight in the low-frequency region, which means the slope tends to be 90°. Although the EIS of HSAC-4 is not the best, it still has small radii and high frequency and it can facilitate quick diffusion of electrolyte ions.

The long cycle stability of HSAC-4 was also tested, as shown in Fig. 5g; the specific capacitance retention is 91.6% after galvanostatic charge-discharge 5000 cycles at a current

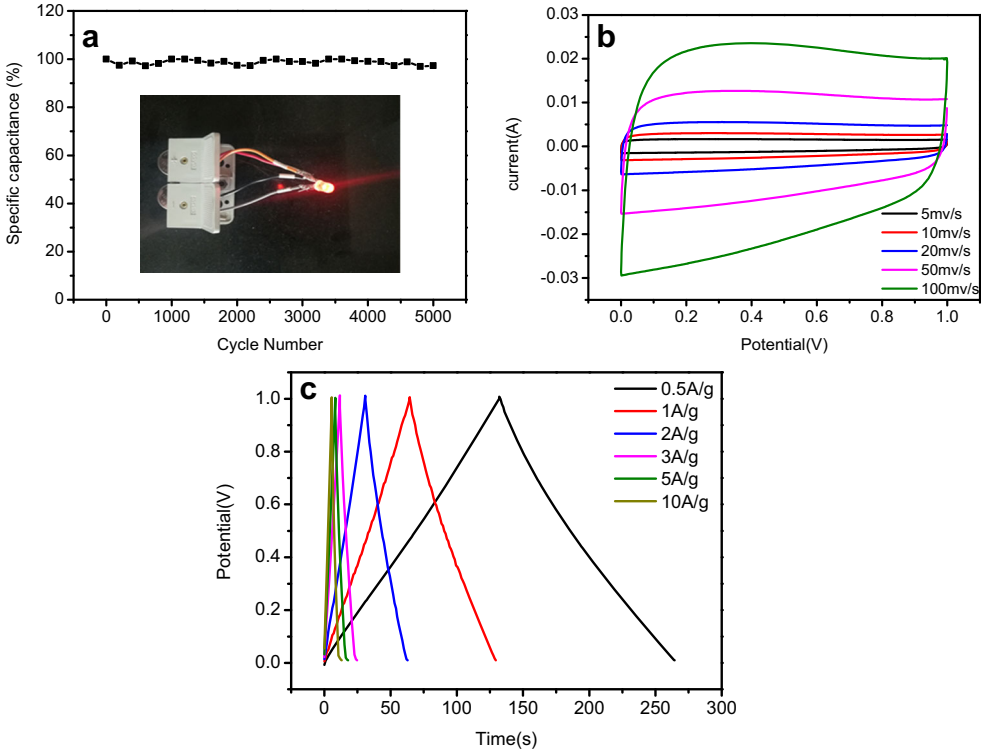

Fig. 6 **a** Cycling stability performance of the all-solid-state device at the current density of 2 A g^{-1} after 5000 cycles. Inset is photograph of lighting LED by the all-solid-state device. **b** CV curves for the all-solid-state device at scan rates ranging from 5 to 100 mV s^{-1}. **c** CP curves of the all-solid-state device at different current densities

density of 2 A g^{-1}, showing an excellent cycling stability. The above analysis shows that the excellent capacitance performance of HSAC-4 can prove it to be used as a supercapacitor electrode material.

In order to explore the practicality of HSACs, a symmetric capacitor device as the all-solid-state supercapacitor device was fabricated with two identical HSAC-4 electrodes (denoted as HSAC-4 // HSAC-4) in 6 mol L^{-1} KOH electrolyte for evaluation. Two all-solid-state supercapacitor devices were connected in series and linked to a commercial LED with a working voltage of 2.7 V. After charged, the HSACs were used as a storage device to light the LED. From the inset of Fig. 6a, it can be seen that the LED is bright when connected to the storage device.

Figure 6b describes the CV curves of HSAC-4 // HSAC-4 device at various scan rates from 5 to 100 mV s^{-1} between 0 and 1 V. Obviously, the CV curves still maintained a rectangular-like shape, indicating that HSAC-4 device has good super capacitance characteristics at different scanning speeds. The charge/discharge curves of HSAC-4 // HSAC-4 device at various current densities (Fig. 6c) were also collected to further evaluate the electrochemical performance. The symmetrical charge/discharge curves indicated a good capacitive performance of the device. According to Eq. (2), the specific capacitance is still at 167 F g^{-1} when the current density varies from 0.5 to 10 A g^{-1}, so HSAC-4 device has stable super capacitance characteristics at different current densities. A very satisfying cycle stability of the HSAC-4 // HSAC-4 device is revealed by Fig. 6a. It shows 97.23% of the primary capacitance preserved after 5000 cycles. From the above results, we can see that HSAC-4 developed in this work can be applied to electrode materials for high-performance liquid and all-solid-state supercapacitors.

Conclusion

Biomass-based active carbon was prepared through the hydrothermal process followed by the carbonization. The prepared electrode material has good capacitance performance with a specific capacitance of 276 F g^{-1} at a current density of 0.5 A g^{-1}. The capacitance retention rate was 91.6% after 5000 cycles at a current density of 2 A g^{-1} showing the material has good cycle stability. As the all-solid-state device, it has certain applications. The preparation method has many advantages, including low toxicological impact of materials and processes, eco-friendly biomaterials, and facile techniques. Therefore, these preparation method materials are promising for further electrochemical applications in supercapacitors.

Funding information This work was supported by the National Key Research and Development Program of China (2016YFC0202900), National Natural Science Foundation of China (21567015), Natural Science Foundation of Gansu Province (17JR5RA109), and Gansu Provincial Party Committee Young Creative Talents (Ganzutongzi, 2017/121).

References

1. Aricò AS, Bruce P, Scrosati B, Tarascon JM, Van Schalkwijk W (2005) Nanostructured materials for advanced energy conversion and storage devices. Nat Mater 4(5):366–377
2. Miller JR, Simon P (2008) Electrochemical capacitors for energy management. Science 321(5889):651–652
3. Shao Y, El Kady MF, Wang LJ, Zhang Q, Li Y, Wang H, Mousavi MF, Kaner RB (2015) ChemInform Abstract: Graphene-Based materials for flexible supercapacitors. Chem Soc Rev 44(30):3639–3665
4. Kötz R, Carlen M (2000) Principles and applications of electrochemical capacitors. Electrochim Acta 45(15):2483–2498
5. Simon P, Gogotsi Y (2010) Charge storage mechanism in nanoporous carbons and its consequence for electrical double layer capacitors. Philos Trans Math Phys Eng Sci 368(1923):3457
6. Ojha K, Kumar B, Ganguli AK (2017) Biomass derived graphene-like activated and non-activated porous carbon for advanced supercapacitors. J Chem Sci 129(3):1–8
7. Ekrami E, Dadashian F, Soleimani M (2014) Waste cotton fibers based activated carbon: Optimization of process and product characterization. Fibers Polym 15(9):1855–1864
8. Zhang G, Xiao X, Li B, Gu P, Xue H, Pang H (2017) Transition metal oxides with one-dimensional/one-dimensional-analogue nanostructures for advanced supercapacitors. J Mater Chem A 5(18):8155–8186
9. Huang GY, Xu SM, Yang Y, Cheng YB, Li J (2016) Preparation of Cobalt-Based Bi-Metal-Oxides and the Application in the Field of Electrochemical Energy Storage. Chinese J Inorg Chem 32(10):1693–1703
10. Shayeh JS, Ehsani A, Ganjali MR, Norouzi P, Jaleh B (2015) Conductive polymer/reduced graphene oxide/Au nano particles as efficient composite materials in electrochemical supercapacitors. Appl Surf Sci 353:594–599
11. Duggal AR, Levinson LM (1997) A novel high current density switching effect in electrically conductive polymer composite materials. J Appl Phys 82(11):5532–5539
12. Wang G, Zhang L, Zhang J (2012) A review of electrode materials for electrochemical supercapacitors. Chem Soc Rev 41(18):797–828
13. Wang Q, Yan J, Fan Z (2016) Carbon materials for high volumetric performance supercapacitors: design, progress, challenges and opportunities. Energy Environ Sci 9(3):729–762
14. Qu D (2002) Studies of the activated carbons used in double-layer supercapacitors. J Power Sources 109(2):403–411
15. Ermakova MA, Ermakov DY, Chuvilin AL, Kuvshinov GG (2001) Decomposition of Methane over Iron Catalysts at the Range of Moderate Temperatures: The Influence of Structure of the Catalytic Systems and the Reaction Conditions on the Yield of Carbon and Morphology of Carbon Filaments. J Catal 201(2):183–197
16. Dupuis AC (2005) The catalyst in the CCVD of carbon nanotubes—a review. Prog Mater Sci 50(8):929–961
17. Pai R, Singh A, Simotwo S, Kalra V (2018) In Situ Grown Iron Oxides on Carbon Nanofibers as Freestanding Anodes in Aqueous Supercapacitors. Adv Eng Mater:170–1116
18. Izadi-Najafabadi A, Yasuda S, Kobashi K, Yamada T, Futaba DN, Hatori H, Yumura M, Iijima S, Hata K (2010) Extracting the Full Potential of Single-Walled Carbon Nanotubes as Durable Supercapacitor Electrodes Operable at 4 V with High Power and Energy Density. Adv Mater 22(35):E235–E241
19. Sun H, Xu Z, Gao C (2013) Aerogels: Multifunctional, Ultra-Flyweight, Synergistically Assembled Carbon Aerogels (Adv. Mater. 18/2013). Adv Mater 25(18):2632
20. Yu X, Cheng H, Zhang M, Zhao Y, Qu L, Shi G (2017) Graphene-based smart materials. Nat Rev Mater 2(17046)
21. Hao P, Zhao Z, Leng Y, Tian J, Sang Y, Boughton RI, Wong CP, Liu H, Yang B (2015) Graphene-based nitrogen self-doped hierarchical porous carbon aerogels derived from chitosan for high performance supercapacitors. Nano Energy 15:9–23
22. Xie Q, Zheng A, Zhai S, Wu S, Xie C, Zhang Y, Guan Y (2016) Reed straw derived active carbon/graphene hybrids as sustainable high-performance electrodes for advanced supercapacitors. J Solid State Electrochem 20(2):449–457
23. Arie AA, Kristianto H, Halim M, Lee JK (2017) Synthesis and modification of activated carbon originated from Indonesian local Orange peel for lithium ion Capacitor's cathode. J Solid State Electrochem 21(5):1–12
24. Zhang J, Gong L, Sun K, Jiang J, Zhang X (2012) Preparation of activated carbon from waste Camellia oleifera shell for supercapacitor application. J Solid State Electrochem 16(6):2179–2186
25. Jiang D, Xiong TY, Fan X, Li MM, Han CL, Gong YT, Wang HY, Yong W (2015) Inspired by bread leavening: one-pot synthesis of hierarchically porous carbon for supercapacitors. Green Chem 17(7):4053–4060
26. Resch G, Held A, Faber T, Panzer C, Toro F, Haas R (2008) Potentials and prospects for renewable energies at global scale. Energ Policy 36(11):4048–4056
27. Wang H, Xu Z, Kohandehghan A, Li Z, Cui K, Tan X, Stephenson TJ, King'Ondu CK, Holt CM, Olsen BC (2013) Interconnected carbon nanosheets derived from hemp for ultrafast supercapacitors with high energy. ACS Nano 7(6):5131–5141
28. Shi G, Liu C, Wang G, Chen X, Li L, Jiang X, Zhang P, Dong Y, Jia S, Tian H (2018) Preparation and electrochemical performance of electrospun biomass-based activated carbon nanofibers. Ionics 1:1–8
29. Li Y, Wei OY, Xu X, Wang M, Hou S, Lu T, Yao Y, Pan L (2018) Micro-/mesoporous carbon nanofibers embedded with ordered carbon for flexible supercapacitors. Electrochim Acta 271:591–598
30. Zhang D, Hao Y, Zheng L, Ma Y, Feng H, Luo H (2013) Nitrogen and sulfur co-doped ordered mesoporous carbon with enhanced electrochemical capacitance performance. J Mater Chem A 1(26):7584–7591
31. Lu SY, Jin M, Zhang Y, Niu YB, Gao JC, Li CM (2017) Chemically Exfoliating Biomass into a Graphene-like Porous Active Carbon with Rational Pore Structure, Good Conductivity, and Large Surface Area for High-Performance Supercapacitors. Adv Energy Mater 1702545
32. Tan Z, Chen G, Zhu Y (2011) Carbon-Based Supercapacitors Produced by the Activation of Graphene. Wiley-Blackwell, pp 211–215
33. Wang R, Wang P, Yan X, Lang J, Peng C, Xue Q (2012) Promising porous carbon derived from celtuce leaves with outstanding supercapacitance and CO_2 capture performance. ACS Appl Mater Interfaces 4(11):5800
34. Thommes M, Kaneko K, Neimark AV, Olivier JP, Rodriguezreinoso F, Rouquerol J, Sing KSW (2011) Physisorption of gases, with special reference to the evaluation of surface area and pore size distribution (IUPAC Technical Report). Chem Int 38(1):25
35. Leal D, Matsuhiro B, Rossi M, Caruso F (2008) FT-IR spectra of alginic acid block fractions in three species of brown seaweeds. Carbohydr Res 343(2):308
36. Jung N, Kwon S, Lee D, Yoon DM, Park YM, Benayad A, Choi JY, Park JS (2013) Synthesis of chemically bonded graphene/carbon nanotube composites and their application in large volumetric capacitance supercapacitors. Adv Mater 25(47):6854–6858
37. Bertóti I, Mohai M, László K (2015) Surface modification of graphene and graphite by nitrogen plasma: Determination of chemical state

alterations and assignments by quantitative X-ray photoelectron spectroscopy. Carbon 84(1):185–196
38. Rantanen J (2007) Process analytical applications of Raman spectroscopy. J Pharm Pharmacol 59(2):171–177
39. Kruk M, Kohlhaas KM, Dufour B, Celer EB, Jaroniec M, Matyjaszewski K, Ruoff RS, Kowalewski T (2007) Partially graphitic, high-surface-area mesoporous carbons from polyacrylonitrile templated by ordered and disordered mesoporous silicas. Microporous Mesoporous Mater 102(1):178–187
40. Li W, Zhang F, Dou Y, Wu Z, Liu H, Qian X, Gu D, Xia Y, Tu B, Zhao D (2011) A Self-Template Strategy for the Synthesis of Mesoporous Carbon Nanofibers as Advanced Supercapacitor Electrodes. Adv Energy Mater 1(3):382–386